

ORIGINAL RESEARCH PAPER

Degradation of Acid Red 18 in an Aqueous Environment by TiO₂/Zeolite Nano Photocatalyst

Aref Shokri^{1,2*}, Safoora Karimi²

¹ Jundi-Shapur research institute, Dezful, Iran

² Department of Chemical Engineering, Jundi-Shapur University of Technology, Dezful, Iran

Received: 2021-06-01

Accepted: 2021-07-26

Published: 2021-08-01

ABSTRACT

In this study, the TiO₂ nanoparticles were supported on Y-type zeolite as a new photocatalyst and used to degrade Acid Red 18 in an aqueous environment. The nano photocatalyst was synthesized by coprecipitation procedure and characterized by Fourier transfer infrared (FTIR), scanning electron microscopy (SEM), and X-ray powder diffraction (XRD). The central composite design (CCD) was employed for the design of the experiment. The effect of operative variables including photocatalyst dosage, contact time, and pH was studied. The ANOVA (analysis of variance) studies displays the second-order regression model with R² = 0.9953, R²pred = 0.9642, R²adj = 0.9910, for the destruction of AR18 was obtained. The contour plots were applied to study the shares of each parameter with mentioned interactions on the degradation of AR18. The optimal circumstances predicted by the model were as the following: the catalyst concentration at 0.88g/L, pH at 6.5, and contact time in 125 min. In this situation, the predicted and actual dye removal were 98.5% and 96.3%, respectively. The removal of COD (chemical oxygen demand) after 125 min was 53% indicating, the notable performance of photocatalyst in mineralization of AR18.

Keywords: TiO₂/Zeolite photocatalyst, Y-type zeolite, Acid Red 18, Central Composite Design, Co-precipitation method.

How to cite this article

Shokri A., Karimi S. Degradation of Acid Red 18 in an Aqueous Environment by TiO₂/Zeolite Nano Photocatalyst. J. Water Environ. Nanotechnol., 2021; 6(4): 326-337.

DOI: 10.22090/jwent.2021.04.004

INTRODUCTION

Currently, many industries including papermaking textiles, printing, tannery, leather, cosmetics ink, and so on, are carrying a high quantity of wasted dye into an aqueous environment [1]. The mentioned dyes make underground and surface waters become painted, producing mutations and carcinogenesis in humans through penetration into them [2]. The removal of azo dyes is one of the significant variables in wastewater treatment. Based on calculations, annually in dye industries, about 15% of the produced dyes are wasted in dyeing and manufacturing processes [3]. Dyes are discharged into an aqueous environment thru several methods; therefore, it is essential to

remove them from their resources [4].

Recently, the Advanced oxidation processes (AOPs) are environmentally friendly and active approaches for the degradation of resistant organic contaminants into intermediate compounds and lastly mineralize them to water and carbon dioxide [5]. The hydroxyl radicals with high oxidation ability were formed by AOPs [6]. Usually, the Heterogeneous photocatalysis approaches are applied to treat the wastewater including refractory organic contaminants, and recycling them because of its capability for complete mineralization of the pollutants at mild circumstances including ambient pressure and temperature.

So far, many different approaches have been suggested for the elimination of dyes from an

* Corresponding Author Email: aref.shokri3@gmail.com

aqueous environment such as the employment of titanium dioxide (TiO_2) nano photocatalyst as one of the most public approaches, with particular restrictions such as needing ultraviolet light [7]. Therefore, a mixture of two photocatalysts has been performed with various methods through doping of non-metals [8], and metals [9], coupling [10], cooping [11-12], and so on; to activate catalyst in the absorption of visible light. By blending two or more semiconducting materials with different energy levels, a new method can activate the photocatalysts under visible light radiation.

Numerous solid semiconductors metal oxides (CeO_2 , TiO_2 , ZrO_2 , Fe_2O_3 , WO_3 , etc.) and sulfides (ZnS , CdS , etc.) have been employed [13–14] for the degradation of chemical substances. Among these photo-catalysts, TiO_2 is the most important due to its unique properties. TiO_2 with different features including, nonhazardous nature, photostable, low operational temperature, availability, low energy consumption, water unsolvability, and high photocatalytic activity at different environmental circumstances stops the production of undesirable by-products [15–16].

Titanium dioxide (TiO_2) nanoparticles due to attractive characteristics including their non-toxic, inexpensive, and biocompatible as well as large special surface area showed the high potential for degradation of azo dyes in wastewater [17]. However, the main disadvantages of utilizing TiO_2 particles in the elimination of azo dyes are agglomeration and coagulation of TiO_2 particles, difficult separation, and reusability of TiO_2 nanoparticles [18]. In recent studies, different kinds of supporting materials such as iron oxide [19], montmorillonite [20], activated carbon, and zeolites [21] were used to enhance the efficiency of TiO_2 nanoparticles for the elimination of dyes from wastewater. Zeolites are microporous, aluminosilicate molecular sieve adsorbents with high ion exchange properties, and higher surface area. Zeolites could be used as efficient supports to prevent the agglomeration of TiO_2 particles in suspension [22]. Chong et al. [21] synthesized TiO_2 -zeolite nanocomposite and the photoactivity of synthesized nanocomposite toward Reactive Black 5 dye degradation was compared with the commercial TiO_2 particles. Ito et al. [23] investigated the adsorption and decomposition of sulfamethazine using high-silica Y-type zeolite- TiO_2 composites. The obtained results showed that the synthesized composites could remove sulfamethazine more effectively compared to

TiO_2 particles. Maraschi et al. [24] studied the simultaneous adsorption and photoactivity of zeolite Y- TiO_2 composites to eliminate enrofloxacin and marbofloxacin from an aqueous environment.

The most extensively used design classes of the response surface method are the Box-Behnken design, CCD, and three-level factorial design. Among these general design classes, CCD is being used for determining the effects of variables on the responses and finally for optimization operations. With the assistance of this method, the effective parameters are being optimized with the minimum number of experimental studies, and at the same time, the interaction among the parameters is also able to be analyzed [25].

Employing a novel synthesized nano photocatalyst by coprecipitation method is the novelty aspect of this process. In the present study, the application of TiO_2/Y zeolite nanocomposite was investigated for degradation of Acid Red 18 from aqueous solutions in a batch system. The catalyst was characterized by XRD, FTIR, and SEM techniques. The effect of functional parameters such as contact time, photocatalyst dosage, and pH on the removal of dye by $\text{TiO}_2/\text{zeolite}$ nano photocatalyst was studied.

EXPERIMENTAL

Materials and apparatus

Acid Red 18, sodium hydroxide, and hydrochloric acid were procured from Merck Company (Germany). Distilled water was used for the preparation of stock solutions. Y-type zeolite (SPX3000) and TiO_2 nanoparticles (Anatase; TiO_2 NPs ~ 30-70 nm) were gained from the Research Institute of Petroleum Industry of Iran (Tehran). The used dye, AR 18, was procured from Alvan Sabet Corporation in Iran and its properties are displayed in Table 1.

The chemical composition of zeolite was obtained by X-ray fluorescence (XRF) analysis which result is listed in Table 2.

The chemical structure of the zeolite and $\text{TiO}_2/\text{zeolite}$ nano photocatalyst was determined using an FTIR spectroscope (Perkin-Elmer Spectrum GX FTIR spectrometer). The XRD patterns of TiO_2 and $\text{TiO}_2/\text{zeolite}$ nano photocatalyst were logged on a Philips instrument, $\text{CuK}\alpha$ radiation (X'pert diffractometer) with a scanning rate of $0.03^\circ \text{ s}^{-1}$ at 25°C . The SEM (MIRA3TESCAN-XMU, SEM) was used for morphological characteristics of prepared nano photocatalyst. A UV-Vis spectrophotometer

Table 1. Features of the AR18.

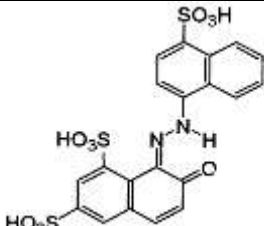
$C_{20}H_{11}N_2Na_3O_{16}S_6$		604.48	505
--------------------------------	---	--------	-----

Table 2. Chemical composition of Y zeolite (SPX3000)

Component	Wt. %
Al ₂ O ₃	10.53
CaO	0.37
SO ₃	0.23
MgO	0.39
K ₂ O	0.26
Fe ₂ O ₃	0.64
BaO	61.30
Na ₂ O	0.53
SiO ₂	25.75

(Perkin Elmer UV-Vis Lambda 25) was applied for recording the spectra and measuring the absorbance of the dye at different operation times.

Preparation of TiO₂/Y zeolite nano photocatalyst

About 5 g of Y-type zeolite particles (SPX3000) were dissolved in 100 mL distilled water and mixed for 1 h. Then, 5 g TiO₂ nanoparticles were added into the zeolite suspension and stirring was sustained for a further 2 h. Then, the precipitant was separated by centrifugation, washed with distilled water, and dried at 80 °C for 10 h. The resultant powder was then calcined at 600 °C for 2 h in the air atmosphere. The obtained adsorbent was stored in a closed bottle for subsequent use.

General Procedure

The photocatalytic degradation of Acid Red 18 using TiO₂/zeolite was performed in batch operation at room temperature. The residual dye concentration was achieved by absorbance measurement at 505 nm, through a UV-VIS spectrophotometer.

The dye conversion (X_d) was used as a process response. The conversion percent as a response was gained by Eq.1, and the removal percent for COD was obtained as (Eq. 2):

$$X_d (\%) = \left(\frac{(AR18)_0 - (AR18)_t}{(AR18)_0} \right) \times 100 \quad (1)$$

$$Removal\ of\ COD (\%) = \left(\frac{(COD)_0 - (COD)_t}{(COD)_0} \right) \times 100 \quad (2)$$

Where (AR18) and (COD) are the concentration of AR18 and amounts of COD at time t, respectively and their amount with zero indexes are the mentioned amounts at the start of the reaction.

Experimental design

For optimizing the removal of AR 18 in synthetic wastewater, the CCD technique was applied. The effect of catalyst dosage, pH, and contact time on the removal of AR 18 was investigated. The input factors with their values were presented in Table 3. The initial concentration of AR18 was fixed at 100 mg/L in all runs.

The RSM was applied to investigate the effect of operational variables on the removal of AR 18[26]. Factor levels are revealed in Table 3 in natural and coded values selected to cover a practical range of variables.

The regression design is being used for modeling the response as a mathematical function.

Table 3. The range and levels of the factors.

Factor	Factor Level				
	-2	-1	0	+1	+2
Catalyst dose(g/l)	0.25	0.5	0.75	1.0	1.25
pH	3	5	7	9	10
Contact time(min)	25	50	75	100	125

Table 4. Design of experiments and actual and predicted values for decolorization of AR18.

Std	Run	A: Catalyst dose(g/l)	B: pH	C: Contact time(min)	Decolorization ⁹
1	17	1.25000	6.5000	75.000	50.5
2	23	0.25000	6.5000	75.000	23.8
3	18	0.75000	6.5000	75.000	58.0
4	4	1.04730	4.4189	45.270	45.5
5	16	0.75000	6.5000	75.000	57.8
6	20	1.04730	4.4189	104.730	83.0
7	8	0.75000	6.5000	75.000	58.3
8	2	0.45270	8.5811	45.270	18.0
9	9	0.75000	10.0000	75.000	51.8
10	12	0.45270	8.5811	104.730	57.0
11	21	0.75000	6.5000	75.000	57.8
12	5	0.75000	6.5000	25.000	19.0
13	22	0.75000	6.5000	75.000	57.9
14	25	0.75000	6.5000	125.000	92.7
15	13	0.45270	4.4189	45.270	26.0
16	7	0.75000	6.5000	75.000	58.2
17	6	1.04730	8.5811	104.730	71.0
18	27	0.45270	4.4189	104.730	66.7
19	29	0.75000	3.0000	75.000	68.0
20	15	1.04730	9.5	45.270	38.0

For emerging the regression equation, the test parameters are coded by the use of the subsequent equation (Eq.3):

$$X_i = \frac{X_i - X_i^x}{\Delta X_i} \quad (3)$$

In this equation, X_i is the actual value of the i th independent variable, x_i is the coded value of the i th independent variable, ΔX_i is the value of step change, and X_i^x is the coded value of the i th independent variable at the center point.

The following relation was attained by the subsequent dimensionless equations (Eq.4):

$$x_1 = A = \frac{C_{D_0} - 700}{200}, x_2 = B = \frac{pH - 6.5}{1.5},$$

$$x_3 = C = \frac{AC - 0.6}{0.2}, x_4 = D = \frac{O_3 - 0.9}{0.3} \quad (4)$$

For controlling the adequacy of the model and estimating the experimental error the replicates were utilized. Generally, the experimental design includes 20 runs (Table 4) in random order to minimize the variability in the response (dye conversion) because of inessential variables.

RESULTS AND DISCUSSION

Characterization of TiO₂/zeolite catalyst

FTIR spectra analysis

The FTIR spectra of zeolite and TiO₂/zeolite nano photocatalyst are demonstrated in Fig. 1. As shown, the zeolite and TiO₂-zeolite nano photocatalyst exhibited the same FTIR spectra features of zeolite which specified the high activity of zeolite as an immobilizer for TiO₂ particles [21]. The wideband at 3420 cm⁻¹ is allocated to O-H stretching for the hydrogen-bonded hydroxyl groups. All undissociated H₂O molecules existing in the materials have a peak at around 1630 cm⁻¹ links to their bending mode. The Al-O-Al or Si-O-Si non-symmetric stretching

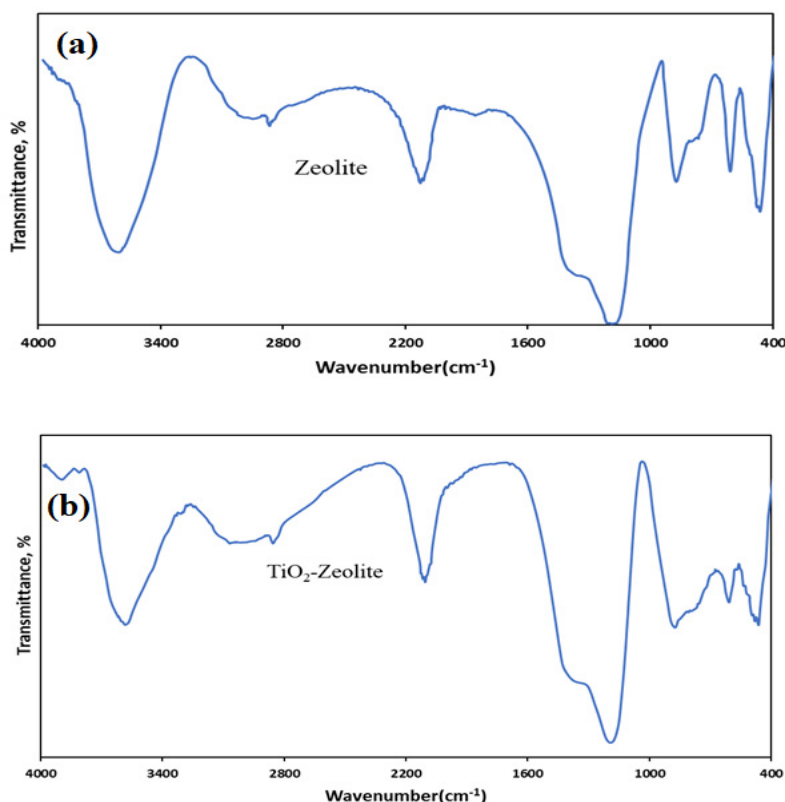


Fig.1. FTIR spectra of zeolite(a), and TiO₂/zeolite nano photocatalyst(b).

vibrations in the zeolite structure have a sharp intense peak at 970 cm⁻¹ [27]. Ti-O-Si non-symmetric stretching can be associated with the 970 cm⁻¹ bands [27]. The higher band intensity of 970 cm⁻¹ is relative to the quantity of Ti existing in the zeolite structure. The absorption band around 447 cm⁻¹ is allocated to the stretching vibrations of the Si-O-Al bands. Two absorption bands that occurred in the 500-800 cm⁻¹ could be attributed to the barium bands of the zeolite framework [28].

XRD analysis

The XRD designs of TiO₂ and TiO₂/zeolite nano photocatalyst are shown in Fig. 2. The peaks at 2θ = 25.3, 37.0, 48.1, 54.3, 56.6, 62., 70.0 and 75.1° link to the anatase phase of the TiO₂ nanoparticles [29]. The presence of new peaks at 2θ = 6.1°, 12.3°, 23.3°, 27.4°, 29.3°, 30.3°, 34.2°, and 38.6° indicated the crystalline structure of Y zeolite. These peaks could be attributed to the barium-aluminosilicate content in the zeolite framework.

SEM images

Fig. 3., represents the FE-SEM images of TiO₂

and TiO₂/zeolite nano photocatalyst. As shown, the particles size of TiO₂ was nearly uniform with an average size of 47 nm (Fig. 3a). Comparison of SEM images of TiO₂ and TiO₂/zeolite nano photocatalyst indicated that the TiO₂ particles for both were morphologically similar and the TiO₂ nanoparticles were dispersed on the surface of the zeolite. The particle size distribution of TiO₂ nanoparticles was in the range of 30-70 nm for both TiO₂ and TiO₂/zeolite composite.

Experimental Design

The influence of three variables such as contact time, pH, and catalyst dosage on the removal of AR 18 are shown in Table 4. The initial concentration of AR18 was fixed at 100 mg/L in all runs.

Table 4 shows the response (conversions of dye) and the subsequent model (Eq. 5) was suggested for the response variable (*Y*) as a polynomial equation of independent factors.

$$Y = \beta_0 + \sum_{i=1}^4 \beta_i x_i + \sum_{i=1}^4 \beta_{ii} x_i^2 + \sum_{i=1}^4 \sum_{j=1, i < j}^4 \beta_{ij} x_i x_j \quad (5)$$

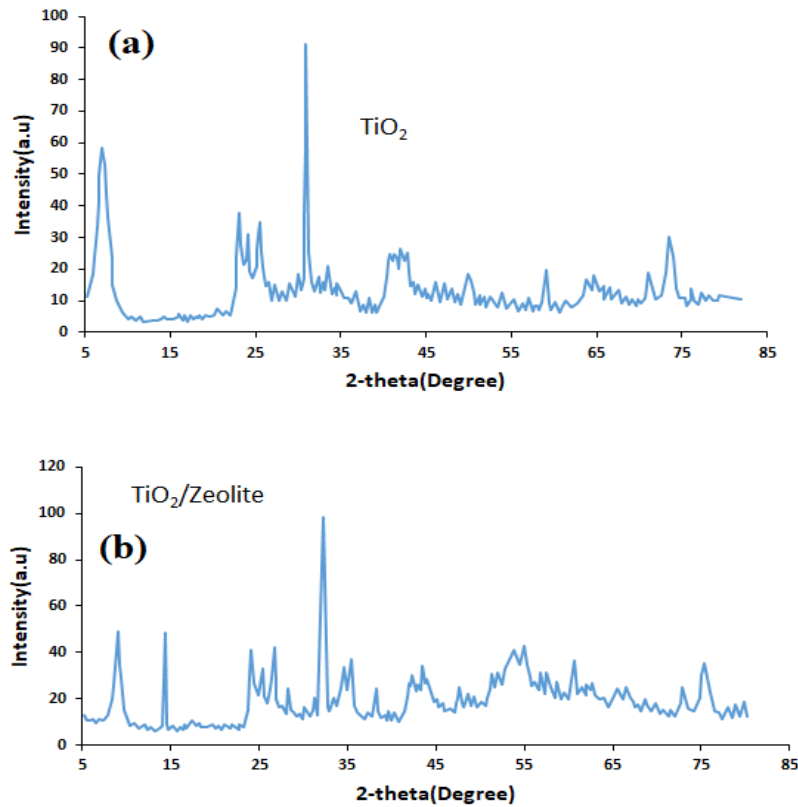


Fig. 2. XRD patterns of TiO₂ (a), and TiO₂/zeolite nano photocatalyst(b).

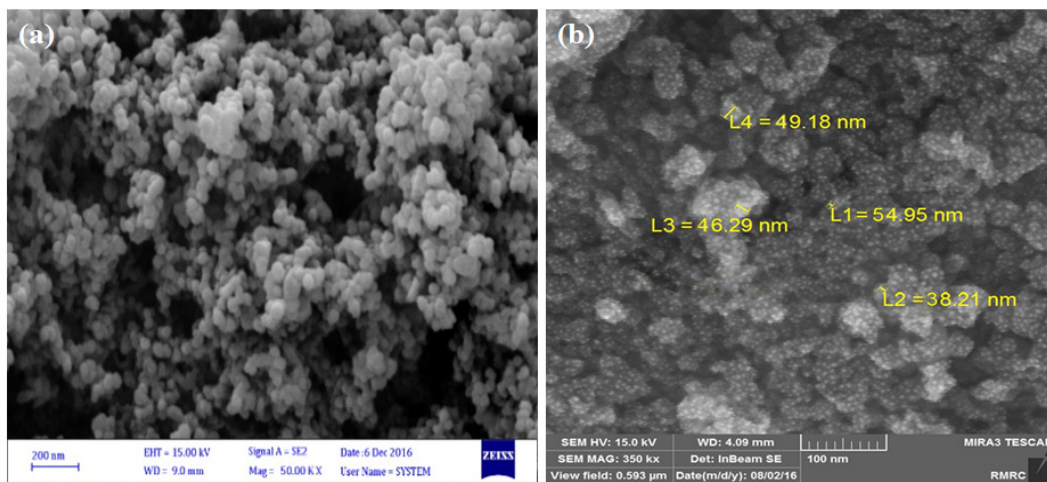


Fig. 3. SEM images of (a) TiO₂ and (b) TiO₂/zeolite nano photocatalyst.

Where Y is the response, the intercept is β_0 , b_i , b_{ij} , and b_{ii} are the linear, pure interaction, and quadratic regression coefficients, respectively, and x_i is the coded independent variables. Due to their good interpolation capability and simple parameter estimation, usually, polynomial models are applied

to interpret the complicated systems due to analysis of parameters easily and good interpolation capability.

Analysis of variance (ANOVA)

The response surface methodology (RSM)

Table 5. ANOVA results in the removal of AR 18 by the photocatalytic process.

Source	Sum of Squares	df	Mean Square	F-value	p-value
Model	7594056	9	843.84	234.57	0.000
Linear	6770.76	3	2256.92	627.37	0.000
A-Catalyst dose	963.4	1	963.4	267.8	0.000
B-pH	304.11	1	304.11	84.53	0.000
C-Contact time	5503.26	1	5503.26	1529.77	0.000
Square	808	3	269.33	74.87	0.000
A ²	778.19	1	778.19	216.32	0.000
B ²	6.96	1	6.96	1.93	0.194
C ²	7.83	1	7.83	2.18	0.171
2-Way interaction	15.79	3	5.26	1.46	0.283
AB	0.41	1	0.41	0.11	0.744
AC	10.58	1	10.58	2.94	0.117
BC	4.81	1	4.81	1.34	0.275
Error	35.97	10	3.6		
Lack of Fit	35.75	5	7.15	162.52	0.000
Pure Error	0.22	5	0.04		
Cor Total	7630.53	19			
	Result				
R ²	0.9882				
Adjusted R ²	0.9910				
Predicted R ²	0.964				
Adeq Precision	31.2822				

was applied to study the influences of operative parameters on dye removal and optimize the method. The design results and complete coding parameter levels are shown in Table 5.

It was clear that the F-value of the model was 234.57, representative of the significance of the model. The P-value of some parameters is fewer than 0.05, their effect on the AR 18 removal is significant. The single factors A, B, and C have significant influences on the removal of AR 18. Based on Table 5, the interactions of AC, AB, BC, C² and B², are not significant (P > 0.05). Thus, the influence of other quadratic forms could be eliminated from the final equation and was not significant [30].

In this model, the F-value related to the lack of fit was 162.52, representing that the lack of fit was not significant. Therefore, the model fitted well with the experimental data, and errors of the tests are low. The values of adjusted R² and R² were achieved to be 0.991 and 0.9882, respectively, representing that the model results were fitted with experimental data. Lastly, these relations display that this model was significant. All of the tests were achieved with various combinations of the variables to study the composing effect of the factors, which were statistically considered based on the CCD.

The factors with no significant interaction were removed from the model to get a final model with significant predictors. Therefore, other significant factors were reserved in the final regression model [31].

According to the experimental results, using the coefficient of the coded variables the predicted second-order polynomial response equation is derived as the following (Eq.6):

$$\begin{aligned} \text{Removal of AR18}(\%) = & -59.0 + 165.1A - \\ & 3.14B + 0.979C - 83.14A^2 + 0.16B^2 - \\ & 0.000834C^2 - 0.36AB - 0.1301AC - 0.0125BC \end{aligned} \quad (6)$$

The Adjusted R² of 0.9910 is in realistic promise with the Predicted R² of 0.964; i.e., the variance is less than 0.2. The signal-to-noise ratio was measured by adequate precision. This ratio was 31.282 shows an adequate signal since a ratio of more than 4 is desirable.

The correlation between actual, and predicted data in AR 18 removal is shown in Fig.4, in which the distribution of data was in a straight line representing that the predicted values were associated by the experimental data of the response. If there is a relationship between the variables and response, then the obtained data should be

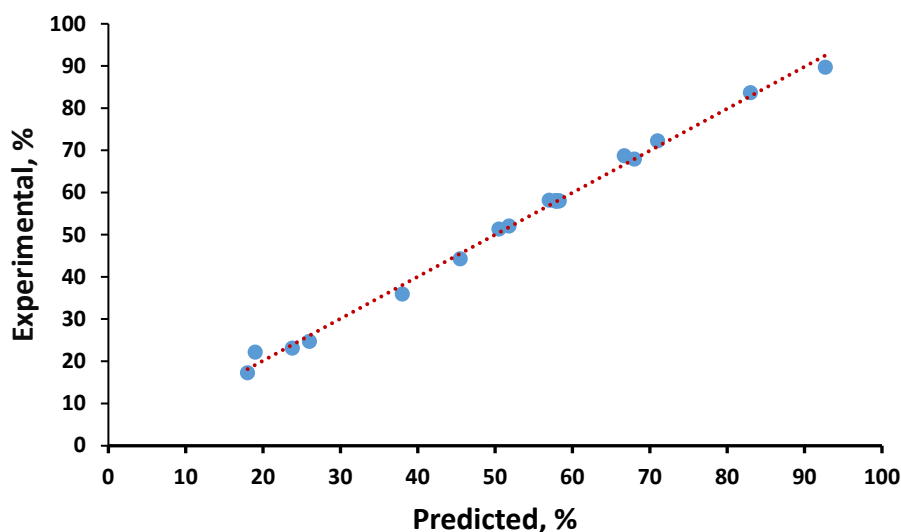


Fig.4. Experimental versus predicted data.

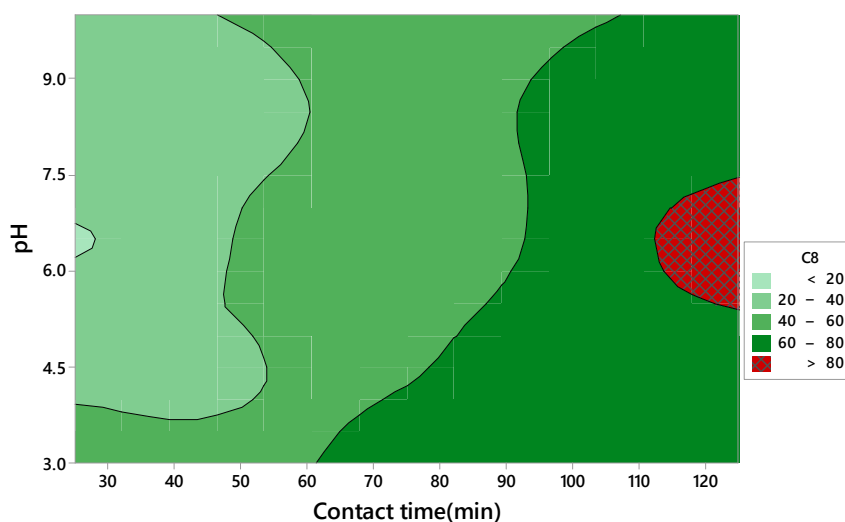


Fig. 5. Effect of pH on degradation of Acid Red 18 using TiO₂/zeolite.

statistically analyzed using regression.

Effect of contact time

The effect of contact time on the Acid Red 18 using TiO₂/zeolite photocatalyst was illustrated in Fig.5. It was clear that, after 120 min of reaction, the degradation of Acid Red 18 was increased to its maximum amounts.

The results verified that there is a positive relation between AR 18 degradation and contact time. Therefore, the removal efficacy of AR 18 was enhanced with an increase in contact time, since by increasing the contact time, the chance of the interaction between the electron-hole pair and AR

18 molecules increased. According to the studies of Rahimi et al., the degradation of Acid Orange 10 enhanced with a rise in contact time, and from the start of the reaction to 150 min, it was increased from 0% to 94% [26]. Other researchers exhibited that, the removal efficacy of tartrazine and Direct Blue 71 was increased with a rise in contact time because the active sites of photocatalyst on the surface of catalyst were increased with increasing the contact time [32].

Effect of the solution pH

The influence of different values of pH on the degradation of AR 18 is illustrated in Fig. 6. The

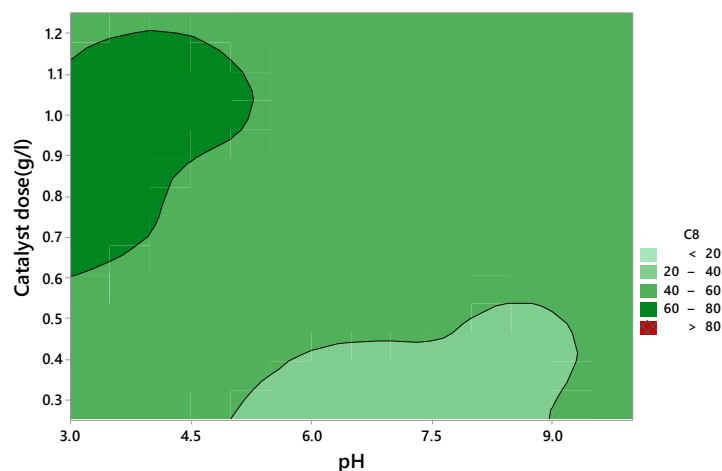


Fig. 6. Effect of pH on degradation of Acid Red 18 using $\text{TiO}_2/\text{zeolite}$.

pH of Acid Red 18 solution is an efficient factor in the photocatalytic process because it impacts the surface charge of the catalyst and the chemistry of the dye molecule consequently on the interaction among adsorbate and the adsorbent. Therefore, the sorption process of Acid Red 18 on $\text{TiO}_2/\text{zeolite}$ nano photocatalyst was performed with different pH values between 3 to 9. The highest value of removal percentage was obtained at a pH range of 6 to 7. This is due to the capability of Y zeolite to form hydrogen bonding with hydronium ions which results in the adsorption of anionic dye on the positive surface of $\text{TiO}_2/\text{zeolite}$ nano photocatalyst. The wonderful reduction of sorption percentage at alkaline pH may be originated from the accumulation of hydroxyl ions on the surface of $\text{TiO}_2/\text{zeolite}$ nano photocatalyst and electrostatic repulsion between negatively charged adsorbent and anionic dye.

The pH had a negative impact on the removal of AR 18 and it was enhanced with reducing pH. The AR 18 removal was enhanced in the acidic pH, based on the strong electrostatic adsorption between the negative charge of the contaminant and the positive charge of the catalyst. So, the attractive forces between AR 18 molecules and the catalyst the rate of AR 18 photodegradation increased [33]. In the present study, the pH_{pzc} of the synthesized photocatalyst was obtained to be 5.5. So, the charge of the catalyst surface would be positive at pH values lower than pH_{pzc} and tend to absorb the negative charge of AR 18.

The photocatalytic degradation of MC-LR with $\text{Ag}/\text{AgCl}/\text{TiO}_2$ as a nano photocatalyst was investigated by Liao et al., and the removal efficacy

was increased with a decrease in the initial pH, based on the attractive forces between pollutant molecules and the catalyst particles [34]. Also, similar research displayed that the elimination of Direct Red 16 was reduced at alkaline pH. Since, at acidic pH, with electrostatic force between the surface of the catalyst and dye molecules, the photocatalytic activity was improved [35].

Effect of catalyst dosage

The influence of photocatalyst dosage on the removal of Acid Red 18 using $\text{TiO}_2/\text{zeolite}$ is shown in Fig.7, and the removal efficacy was increased by increasing the adsorbent amount. Because in the high concentration of catalyst, the active sites on catalysts surface were increased to get more photons, which result in the production of more superoxide and hydroxyl radicals, and subsequently, degradation of more AR18 molecules.

Some researchers found that the degradation of Methylene Blue and tartrazine increased with an increase in the catalyst dosage. Because the photocatalytic active sites were increased with an increase in catalyst dose and more photons were adsorbed, and afterward, more hydroxyl and superoxide radicals were produced, resulting in more pollutant degradation [36].

Optimum conditions

For optimization of AR18 removal, the values of various factors were attained through Design-Expert software, version 7.0. The optimum values and the percentage of AR18 removal are presented in Table 6. As it is clear, the optimal circumstances predicted by the model were as the following:

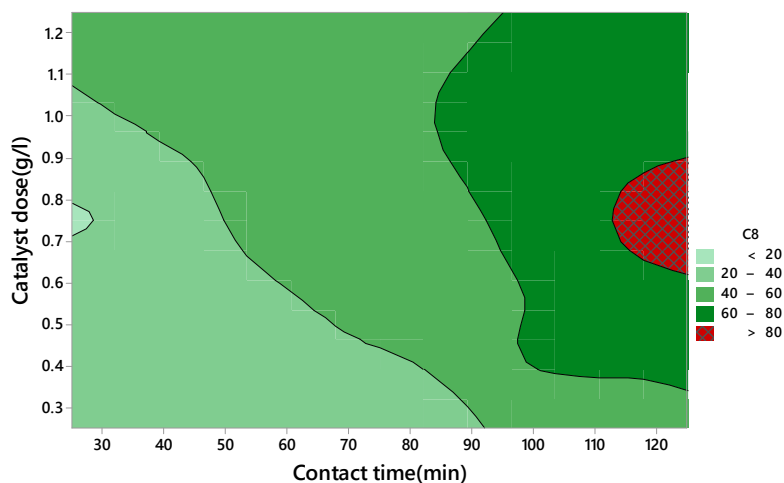
Fig. 7. Effect of pH on degradation of Acid Red 18 using TiO₂/zeolite.

Table 6. Optimum conditions in the removal of AR18.

Parameters	Unit	Value
catalyst concentration	g/L	0.88
contact time	min	125
pH	-	6.5
Predicted AR18 removal	%	98.5
Experimental AR18 removal	%	96.3

the catalyst concentration at 0.88 g/L, pH at 6.5, and contact time in 125 min. In this situation, the predicted and actual dye removal was 98.5% and 96.3%, respectively. At optimum conditions, the removal of COD was 53%, and the COD was decreased from 300 to 140 mg/L.

CONCLUSION

In this study, the performance of TiO₂/Zeolite (Y type) nano photocatalyst was studied for photocatalytic degradation of Acid Red 18 in a batch mode. The nano photocatalyst was synthesized by coprecipitation technique and characterized by FTIR, XRD, and FE-SEM techniques.

The XRD and FTIR patterns of TiO₂ and TiO₂/zeolite composite indicated the successful blending of TiO₂ and zeolite particles without chemical interaction between TiO₂ and zeolite particles. SEM images of prepared nanoparticles indicated that both TiO₂ and TiO₂/zeolite composite were morphologically similar.

The CCD was used for experimental design and the second-order regression model. The influences of operating variables including contact time, photocatalyst dosage, and pH were studied. The contour plots were used to study the parts of each

factor, and their interactions on the degradation of AR18. The optimum conditions predicted by the model were the catalyst concentration at 0.88 g/L, pH at 6.5, and contact time in 125 min. The predicted and actual removal of dye were 96.3% and 98.5%, respectively. The removal of COD after 125 min was 53% indicating the notable performance of photocatalyst in mineralization of AR18.

CONFLICTS OF INTEREST

There are no conflicts to declare.

REFERENCES

1. M. Soniya, G. Muthuraman, Removal and recovery of malachite green and methyl violet dyes from textile wastewater using 2-nitrobenzoic acid as an extractant, *Int. J. Chem-tech Res.* 7 (2015) 3046-3050.
2. Alves de Lima RO, Bazo AP, Salvadori DMF, Rech CM, de Palma Oliveira D, de Aragão Umbuzeiro G. Mutagenic and carcinogenic potential of a textile azo dye processing plant effluent that impacts a drinking water source. *Mutation Research/Genetic Toxicology and Environmental Mutagenesis.* 2007;626(1-2):53-60.
3. Couch RL, Price JT, Fatehi P. Production of Flocculant from Thermomechanical Pulping Lignin via Nitric Acid Treatment. *ACS Sustainable Chemistry & Engineering.* 2016;4(4):1954-62.
4. Rajabi HR, Arjmand H, Hoseini SJ, Nasrabadi H. Surface

- modified magnetic nanoparticles as efficient and green sorbents: Synthesis, characterization, and application for the removal of anionic dye. *Journal of Magnetism and Magnetic Materials*. 2015;394:7-13.
5. Shokri A. A kinetic study and application of electro-Fenton process for the remediation of aqueous environment containing toluene in a batch reactor. *Russian Journal of Applied Chemistry*. 2017;90(3):452-7.
 6. Bayat A, Shokri A. Degradation of p-Nitrotoluene in aqueous environment by Fe(II)/Peroxymonosulfate using full factorial experimental design. *Separation Science and Technology*. 2020;56(17):2941-50.
 7. Rahimi B, Ebrahimi A. Photocatalytic process for total arsenic removal using an innovative BiVO₄/TiO₂/LED system from aqueous solution: Optimization by response surface methodology (RSM). *Journal of the Taiwan Institute of Chemical Engineers*. 2019;101:64-79.
 8. Joseph AIJ, Thiripuranthagan S. Non-Metal Doped Titania Photocatalysts for the Degradation of Neonicotinoid Insecticides Under Visible Light Irradiation. *Journal of Nanoscience and Nanotechnology*. 2018;18(5):3158-64.
 9. Ünlü B, Çakar S, Özacar M. The effects of metal doped TiO₂ and dithizone-metal complexes on DSSCs performance. *Solar Energy*. 2018;166:441-9.
 10. Sharma H, Mahajan H, Jamwal B, Paul S. Cu@Fe₃O₄-TiO₂-L-dopa: A novel and magnetic catalyst for the Chan-Lam cross-coupling reaction in ligand free conditions. *Catalysis Communications*. 2018;107:68-73.
 11. Kang K, Yan J, Zhang J, Du J, Yi J, Liu Y, et al. (Ge, GeO₂, Ta₂O₅, BaCO₃) co-doping TiO₂ varistor ceramics. *Journal of Alloys and Compounds*. 2015;649:1280-90.
 12. Song W, Zhao H, Wang L, Liu S, Li Z. Co-doping Nitrogen/Sulfur through a Solid-State Reaction to Enhance the Electrochemical Performance of Anatase TiO₂ Nanoparticles as a Sodium-Ion Battery Anode. *ChemElectroChem*. 2017;5(2):316-21.
 13. Cha BJ, Saqlain S, Seo HO, Kim YD. Hydrophilic surface modification of TiO₂ to produce a highly sustainable photocatalyst for outdoor air purification. *Applied Surface Science*. 2019;479:31-8.
 14. Sun X, Yan L, Xu R, Xu M, Zhu Y. Surface modification of TiO₂ with polydopamine and its effect on photocatalytic degradation mechanism. *Colloids and Surfaces A: Physicochemical and Engineering Aspects*. 2019;570:199-209.
 15. Shokri A, Joshagani AH. Using microwave along with TiO₂ for degradation of 4-chloro-2-nitrophenol in aqueous environment. *Russian Journal of Applied Chemistry*. 2016;89(12):1985-90.
 16. Abdullah H, Khan MMR, Ong HR, Yaakob Z. Modified TiO₂ photocatalyst for CO₂ photocatalytic reduction: An overview. *Journal of CO₂ Utilization*. 2017;22:15-32.
 17. Janus M, Kusiak-Nejman E, Morawski AW. Determination of the photocatalytic activity of TiO₂ with high adsorption capacity. *Reaction Kinetics, Mechanisms and Catalysis*. 2011;103(2):279-88.
 18. Shokri A, Mahanpoor K. Degradation of ortho-toluidine from aqueous solution by the TiO₂/O₃ process. *International Journal of Industrial Chemistry*. 2016;8(1):101-8.
 19. M Rostami, H Mazaheri, A Hassani Joshaghani, A Shokri, Using Experimental Design to Optimize the Photo-degradation of P-Nitro Toluene by Nano-TiO₂ in Synthetic Wastewater, *Int. J. Eng.*, 32 (8), 1074-1081.
 20. Djellabi R, Ghorab MF, Cerrato G, Morandi S, Gatto S, Oldani V, et al. Photoactive TiO₂-montmorillonite composite for degradation of organic dyes in water. *Journal of Photochemistry and Photobiology A: Chemistry*. 2014;295:57-63.
 21. Chong MN, Tneu ZY, Poh PE, Jin B, Aryal R. Synthesis, characterisation and application of TiO₂-zeolite nanocomposites for the advanced treatment of industrial dye wastewater. *Journal of the Taiwan Institute of Chemical Engineers*. 2015;50:288-96.
 22. Ito M, Fukahori S, Fujiwara T. Adsorptive removal and photocatalytic decomposition of sulfamethazine in secondary effluent using TiO₂-zeolite composites. *Environmental Science and Pollution Research*. 2013;21(2):834-42.
 23. A Shokri, K Mahanpoor, Removal of Ortho-Toluidine from Industrial Wastewater by UV/TiO₂ Process, *J Chem Health Risk (JCHR)* 6 (3), 213-223.
 24. Maraschi F, Sturini M, Speltini A, Pretali L, Profumo A, Pastorello A, et al. TiO₂-modified zeolites for fluoroquinolones removal from wastewaters and reuse after solar light regeneration. *Journal of Environmental Chemical Engineering*. 2014;2(4):2170-6.
 25. Varank G, Yazici Guvenc S, Dincer K, Demir A. Concentrated Leachate Treatment by Electro-Fenton and Electro-Persulfate Processes Using Central Composite Design. *International Journal of Environmental Research*. 2020;14(4):439-61.
 26. Rahimi B, Jafari N, Abdolhnejad A, Farrokhzadeh H, Ebrahimi A. Application of efficient photocatalytic process using a novel BiVO₄/TiO₂-NaY zeolite composite for removal of acid orange 10 dye in aqueous solutions: Modeling by response surface methodology (RSM). *Journal of Environmental Chemical Engineering*. 2019;7(4):103253.
 27. Chong MN, Tneu ZY, Poh PE, Jin B, Aryal R. Synthesis, characterisation and application of TiO₂-zeolite nanocomposites for the advanced treatment of industrial dye wastewater. *Journal of the Taiwan Institute of Chemical Engineers*. 2015;50:288-96.
 28. A. Gamba, C. Colella, S. Coluccia, Effect of Ti insertion in the silicalite framework on the vibrational modes of the structure: an ab initio, and vibrational study (2001).
 29. Aronne A, Esposito S, Ferone C, Pansini M, Pernice P. FTIR study of the thermal transformation of barium-exchanged zeolite A to celsian. *Journal of Materials Chemistry*. 2002;12(10):3039-45.
 30. A Shokri, Removal of Acid red 33 from aqueous solution by Fenton and photo Fenton processes, *J Chem Health Risk (JCHR)* 7 (2), 119-131.
 31. Shokri A, Karimi S. Treatment of Aqueous Solution Containing Acid red 14 using an Electro Peroxone Process and a Box-Behnken Experimental Design. *Archives of Hygiene Sciences*. 2020;9(1):48-57.
 32. Shokri A. Investigation of UV/H₂O₂ process for removal of ortho-toluidine from industrial wastewater by response surface methodology based on the central composite design. *DESALINATION AND WATER TREATMENT*. 2017;58:258-66.
 33. Rahimi B, Jafari N, Abdolhnejad A, Farrokhzadeh H, Ebrahimi A. Application of efficient photocatalytic process using a novel BiVO₄/TiO₂-NaY zeolite composite for removal of acid orange 10 dye in aqueous solutions: Modeling by response surface methodology (RSM). *Journal of Environmental Chemical Engineering*. 2019;7(4):103253.
 34. Arabzadeh N, Mohammadi A, Darwish M, Abuzerr S.

- Construction of a TiO₂-Fe₃O₄-decorated molecularly imprinted polymer nanocomposite for tartrazine degradation: Response surface methodology modeling and optimization. *Journal of the Chinese Chemical Society*. 2018;66(5):474-83.
35. Jafari N, Ebrahimpour K, Abdolahnejad A, Karimi M, Ebrahimi A. Efficient degradation of microcystin-LR by BiVO₄/TiO₂ photocatalytic nanocomposite under visible light. *J Environ Health Sci Eng*. 2020;17(2):1171-83.
36. Liao W, Zhang Y, Zhang M, Murugananthan M, Yoshihara S. Photoelectrocatalytic degradation of microcystin-LR using Ag/AgCl/TiO₂ nanotube arrays electrode under visible light irradiation. *Chemical Engineering Journal*. 2013;231:455-63.
37. Zangeneh H, Farhadian M, Zinatizadeh AA. N (Urea) and C N (L-Asparagine) doped TiO₂-CuO nanocomposites: Fabrication, characterization and photodegradation of direct red 16. *Journal of Environmental Chemical Engineering*. 2020;8(1):103639.
38. Koh PW, Yuliati L, Lee SL. Kinetics and Optimization Studies of Photocatalytic Degradation of Methylene Blue over Cr-Doped TiO₂ using Response Surface Methodology. *Iranian Journal of Science and Technology, Transactions A: Science*. 2017;43(1):95-103.